Available online at www.sciencedirect.com
SCIENCE DIRECT
Journal of Catalysis 229 (2005) 30–44
JOURNAL OF CATALYSIS
www.elsevier.com/locate/jcat

The chemical and electronic properties of oxygen-modified C/Mo(110): a model system for molybdenum oxycarbides

Henry H. Hwu [a], Michael B. Zellner [a], Jingguang G. Chen [b,*]

[a] *Department of Materials Science and Engineering, Center for Catalytic Science and Technology (CCST), University of Delaware, Newark, DE 19716, USA*
[b] *Department of Chemical Engineering, Center for Catalytic Science and Technology (CCST), University of Delaware, Newark, DE 19716, USA*

Received 13 January 2004; revised 3 September 2004; accepted 13 September 2004

Abstract

We have utilized oxygen-modified C/Mo(110) surfaces as model systems to determine the modification effect of oxygen in "oxycarbides." Using cyclohexene, ethylene, and methanol as probe molecules, we observed that the reactivity of the O/C/Mo(110) surfaces depended strongly on the temperature at which oxygen was introduced onto the C/Mo(110) surface. The reaction pathways were determined using both temperature-programmed desorption (TPD) and high-resolution electron energy loss spectroscopy (HREELS). For example, the O/C/Mo(110) surface obtained by exposing the carbide surface to oxygen at 600 K became chemically inert toward all three molecules. On the other hand, the 900 K O/C/Mo(110) surface was active toward all three molecules, and for the most part retained the Pt-like reaction pathways observed on unmodified C/Mo(110). Furthermore, we have also compared the electronic properties of the O/C/Mo(110) surfaces using two synchrotron spectroscopies, soft X-ray photoelectron spectroscopy (SXPS) and near-edge X-ray absorption fine structure (NEXAFS); the results revealed similar electronic properties between the 900 K O/C/Mo(110) and unmodified C/Mo(110) surfaces.
© 2004 Elsevier Inc. All rights reserved.

Keywords: C/Mo(110); O/C/Mo(110); SXPS; NEXAFS; DFT; Carbides; Oxycarbides

1. Introduction

It has been well documented that early transition metal (Groups IV–VIB) carbides, when compared to their parent metals, often exhibit catalytic properties that are similar to those of Pt-group metals [1,2]. For example, in our previous surface science studies we have demonstrated that the surface reactivities of carbide-modified V(110) [3,4], Mo(110) [5–7], W(111) [8,9], W(110) [10,11], and Ti(0001) [12] are often very similar to those of the Pt(111) surface.

For catalytic reactions, the surfaces of carbide materials are often oxidized by air or by oxygen-containing reactants or products. Several research groups have reported that the reactivity of carbides can be significantly modified by the presence of oxygen [13–15]. For example, Iglesia and co-workers have reported that unmodified tungsten carbide catalysts were active toward the dehydrogenation of alkanes and the hydrogenation of alkenes [13]. The presence of chemisorbed oxygen on these surfaces, however, directed the catalytic selectivity toward isomerization and dehydration pathways, which were not observed on the unmodified surface [13,14]. These oxygen-modified carbides, or "oxycarbides," were characterized as bifunctional in their ability to catalyze both dehydrogenation and carbenium-ion reactions [13].

We have recently investigated the effect of oxygen modification on the surface reactivity of carbide-modified W(111) [9,16]. We found that the reactivity of the oxygen-modified C/W(111) surfaces depended strongly on the surface temperature at which oxygen was introduced. The C/W(111) surface, after exposure to oxygen at 900 K, or 900 K O/C/W(111), retained the Pt-like reactivity toward cyclohexene. On the other hand, the C/W(111) surfaces that were exposed to oxygen at 600 or 100 K were nearly inert [9]. Ad-

* Corresponding author.
E-mail address: jgchen@udel.edu (J.G. Chen).

0021-9517/$ – see front matter © 2004 Elsevier Inc. All rights reserved.
doi:10.1016/j.jcat.2004.09.014

ditional vibrational spectroscopic studies revealed that when introduced at 600 or 100 K, the atomic and/or molecular oxygen occupied the on-top sites of the C/W(111) surface. In contrast, the vibrational results on the 900 K O/C/W(111) surface suggested that the oxygen atoms did not occupy the on-top sites, which would enable the cyclohexene to interact more strongly with the surface [9]. Using methanol as a probe molecule, the 900 K O/C/W(111) surface appeared to be less active toward C–O bond scission than C/W(111), as evidenced by its increased selectivity toward the production of gas-phase CO [17].

In this paper we report the effect of oxygen modification on C/Mo(110). We have used several types of probe molecules, including linear olefin (ethylene), cyclic olefin (cyclohexene), and oxygenate (methanol) to investigate the activity of oxygen-modified C/Mo(110), or O/C/Mo(110). In addition, we have utilized several electron spectroscopies, including soft X-ray photoelectron spectroscopy (SXPS) and near-edge X-ray absorption fine structure (NEXAFS) to compare the electronic properties of the C/Mo(110) and O/C/Mo(110) surfaces.

For the purpose of comparison, we will briefly summarize our previous studies of the reactions of cyclohexene [6,7], ethylene [5], and methanol [17] on unmodified C/Mo(110). Cyclohexene adsorbed via a di-σ configuration on C/Mo(110), and subsequently dehydrogenated to produce gas-phase benzene. Quantitative analysis revealed that approximately 70% of the adsorbed cyclohexene underwent selective dehydrogenation to produce benzene [6,7]. In the reaction of ethylene, HREEL studies following the low-temperature adsorption of ethylene showed vibrational spectra features consistent with those of the ethylidyne intermediate (CCH_3) when the overlayer was heated to 260 K [5]. Both the selective hydrogenation of cyclohexene to benzene and the conversion of ethylene to ethylidyne were strong indications that the surface reactivity of Mo(110) became "Pt-like" upon carbide modification [2]. Finally, studies probing the interaction of methanol on C/Mo(110) revealed the formation of a stable methoxy intermediate at temperatures between 120 and 330 K [17].

2. Experimental

2.1. Techniques

One of the ultrahigh vacuum (UHV) chambers used in the current study was located at the University of Delaware, and has been described in detail previously [5]. Briefly, it was a three-level stainless-steel chamber equipped with Auger electron spectroscopy (AES) and temperature-programmed desorption (TPD) in the top two levels, and high-resolution electron energy loss spectroscopy (HREELS) in the bottom level. The HREEL spectra reported here were acquired with a primary beam energy of 6 eV. Angles of incidence and reflection were 60° with respect to the surface normal in the on-specular direction. Intensities of the elastic peak were typically in the range of 3×10^4 to 3×10^5 counts per second, and the spectral resolution was between 40 and 55 cm^{-1} FWHM (full width at half-maximum). For TPD and HREELS experiments the Mo(110) sample was heated with a linear heating rate of 3 K/s.

The NEXAFS and SXPS experiments were conducted at the U1A and U12A beamlines, respectively, at the National Synchrotron Light Source (NSLS) of Brookhaven National Laboratory. These beamlines and their respective UHV end stations have been previously described in detail [18,19]. SXPS data were recorded on U12A with an incident energy of 150 eV for the Mo valence states [18]; each spectrum represented the average of 10 consecutive scans. The binding energy of each spectrum was then calibrated based on the Fermi energy. The end station contained a VSW EA125 electrostatic analyzer, which was set to operate in constant pass energy mode (10 eV) for photoemission measurements. The instrument resolution was better than 0.5 eV for all spectra. The carbon *K*-edge NEXAFS spectra were recorded on U1A by measuring partial electron yield using a channeltron multiplier located near the sample surface [19]. Both UHV chambers were equipped with an Auger electron spectrometer and a UTi quadrupole mass spectrometer to ensure identical experimental conditions with the UHV chamber at the University of Delaware.

The single crystal sample was a (110) oriented, 1.5-mm-thick molybdenum disk (99.999%), 10 mm in diameter, and was purchased from Metal Crystals and Oxides, Ltd., Cambridge, England. The crystal was spot welded directly to two tantalum posts that served as electrical connections for resistive heating, as well as thermal contacts for cooling with liquid nitrogen. With this mounting scheme, the temperature of the crystal could be varied between 90 and 1200 K. Cyclohexene (Aldrich, 99% purity) and methanol (Aldrich, 99+% purity) were purified by successive freeze–pump–thaw cycles prior to their use. Ethylene (99.99% purity) and oxygen (99.99% pure) were obtained from Matheson and were used without further purification. The purity of the above gases was verified in situ by mass spectrometry. In all experiments, the gas exposures were made at a crystal temperature of 120 K with the crystal located in front of the leak valve. The gas exposures were made by backfilling the vacuum chamber. Doses are reported in Langmuirs (1.0 Langmuir (L) $= 1 \times 10^{-6}$ Torr s) and are uncorrected for ion gauge sensitivity.

2.2. Preparation of C/Mo(110) and O/C/Mo(110)

A clean Mo(110) crystal surface was prepared by cycles of Ne^+ bombardment at 500 K (sample current ~ 5 μA) and flashing to 1150 K. These 5-min cycles were generally repeated 3 times before annealing at 1150 K. To remove carbon contamination, excess O_2 was used to react with carbide layers at 900 K. This oxygen treatment process was repeated several times to remove both surface and bulk carbon. Auger

analysis showed that the C and O impurities were both less than 1% of a monolayer after the above cleaning procedure.

Carbide-modified Mo(110), or C/Mo(110), was prepared using ethylene as a carbon source, as described previously [5–7]. In brief, clean Mo(110) was exposed to saturation coverage of ethylene at 600 K and then flashed to 1150 K; generally these procedures were repeated for 3 cycles. The Auger C(KLL)/Mo(MNN) ratio was typically between 0.20 and 0.23, which corresponded to an atomic C/Mo ratio approximately between 0.40 and 0.46 based on the standard AES sensitivity factors [20]. The oxygen-modified C/Mo(110) surfaces were prepared by exposing C/Mo(110) to 7.0 L of O_2 at either 600 or 900 K. The atomic C/Mo and O/Mo ratios for the 600 K O/C/Mo(110) surface were 0.36 and 0.44, respectively. On the 900 K O/C/Mo(110) surface, the atomic C/Mo and O/Mo ratios were 0.31 and 0.08, respectively.

3. Results and interpretation

3.1. HREELS and TPD characterization of the O/C/Mo(110) surfaces

Fig. 1 compares the HREEL spectra of the various oxygen and carbide-modified Mo(110) surfaces. The bottom HREEL spectrum shows the vibrational spectrum of C/Mo(110). The peak at 386 cm^{-1} has been assigned to the ν(Mo–C) mode in previous studies [5–7]. The vibrational spectrum of O/Mo(110), prepared by dosing 30 L of oxygen on clean Mo(110) at 600 K, is shown at the top. Based on previous studies of oxygen on other early transition metals, the 433 and 595 cm^{-1} modes are typically assigned to the deformation and stretching Mo–O modes, respectively, of atomic oxygen on the surface bridging sites [9,21–23]. The 988 cm^{-1} feature is typically attributed to the ν(Mo–O) mode of atomic oxygen in an on-top site or subsurface site [9,21–23].

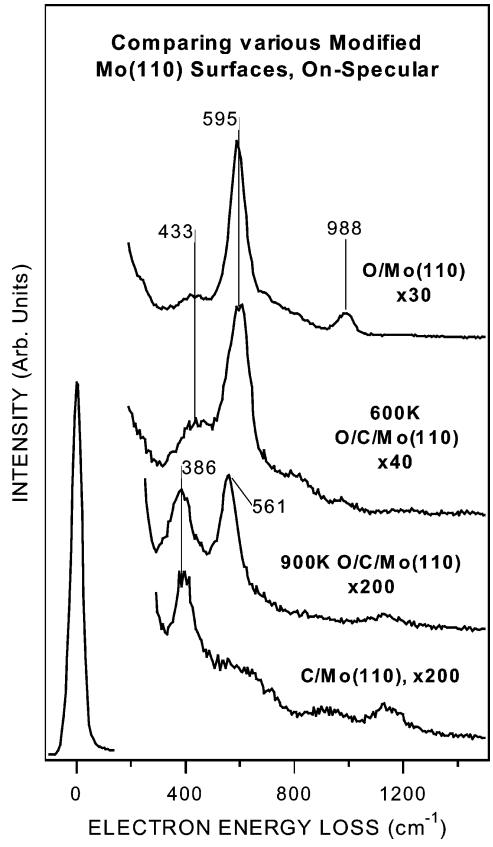

Fig. 1. HREEL spectra comparing various chemically modified Mo(110) surfaces.

In comparison, the HREEL spectrum of the 600 K O/C/Mo(110) surface strongly resembles that of the O/Mo(110) surface. The dominant vibrational modes at 433 and 595 cm^{-1} are similarly assigned to the δ(Mo–O) and ν(Mo–O) modes of atomic oxygen on the bridging sites, respectively. In addition, the 433 cm^{-1} feature on the 600 K O/C/Mo(110) surface is more intense than that on O/Mo(110), which maybe attributed to the overlapping with the ν(Mo–C) mode in the same frequency range. In contrast, the 900 K O/C/Mo(110) surface is characterized by two well-resolved features at 386 and 561 cm^{-1}, which are much weaker in intensity as compared to the features on 600 K O/C/Mo(110) (as indicated by the fivefold difference in the multiplication factors). The 386 cm^{-1} peak is most likely a mixture of the ν(Mo–C) and δ(Mo–O) modes, while the 561 cm^{-1} peak is the ν(Mo–O) mode of atomic oxygen occupying the bridging sites. The significant differences in the lineshape and vibrational frequencies of the ν(Mo–O) modes suggest that oxygen atoms are occupying bridging sites with different binding environments on the 600 and 900 K O/C/Mo(110) surfaces.

Fig. 2 compares the recombinative CO desorption, i.e., recombination of surface atomic C and O, from the 600 and 900 K O/C/Mo(110) surfaces. The desorption of CO from the 600 K O/C/Mo(110) surface is characterized by a peak centered at 760 K, followed by another more intense peak at 913 K. On the 900 K O/C/Mo(110), one CO desorption is detected at 973 K, with another feature at $\sim$ 1056 K. The different desorption temperatures again suggest that oxygen atoms are most likely occupying sites with different binding environment on the two O/C/Mo(110) surfaces.

3.2. Chemical reactivities of the 600 and 900 K O/C/Mo(110) surfaces

3.2.1. Decomposition and dehydrogenation of cyclohexene

Fig. 3 compares the TPD spectra of mass 2 (hydrogen), mass 67 (a major cracking pattern of cyclohexene), and mass 78 (benzene) obtained following 3.0 L exposures of cyclohexene on the 600 and 900 K O/C/Mo(110) surfaces. The spectra recorded from unmodified C/Mo(110) are also included for comparison. As shown in Fig. 3a, the molecular desorption of cyclohexene (mass 67) on 900 K O/C/Mo(110) is observed at 211 K, which is slightly more intense than

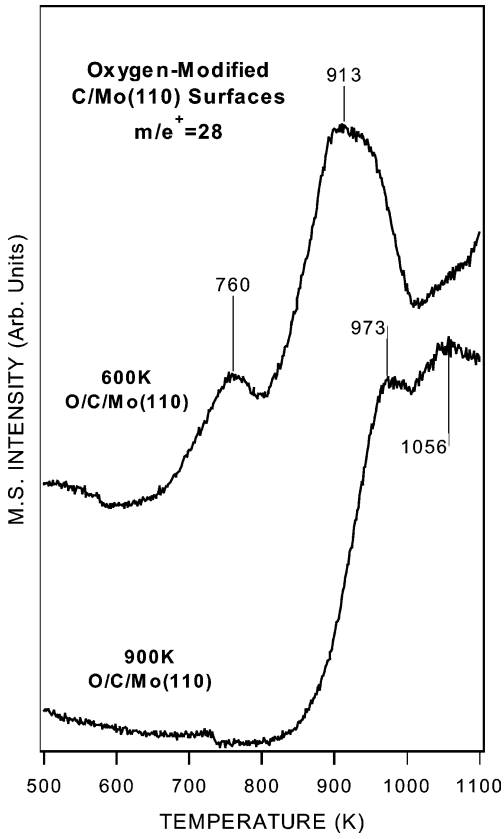

Fig. 2. TPD spectra monitoring the CO desorption from heating the 600 and 900 K O/C/Mo(110).

that from unmodified C/Mo(110). Fig. 3b shows a broad hydrogen desorption peak centered at 381 K on the 900 K O/C/Mo(110) surface; it is slightly lower in temperature than the broad peak at 400 K from C/Mo(110). As shown in Fig. 3c, a benzene feature is observed at 284 K on the 900 K O/C/Mo(110) surface, which is visibly weaker and at lower in temperature than the benzene peak on the unmodified C/Mo(110) surface.

In contrast, the desorption of hydrogen is not detected from the 600 K O/C/Mo(110) surface, indicating that the surface is inactive toward the decomposition or dehydrogenation of cyclohexene. The observation of an intense molecular cyclohexene desorption at 211 K also confirms that the surface is inert. It is important to note that the 211 K peak in the mass 78 spectrum is attributed to the cracking pattern of molecularly desorbed cyclohexene at the same temperature.

As was determined in prior studies [6,7], cyclohexene on C/Mo(110) undergoes either complete decomposition to produce surface C and gas-phase H_2 ($\sim$ 33% selectivity) or selective dehydrogenation to benzene (67% selectivity). Based on the relative peak intensities of hydrogen, cyclohexene, and benzene in Fig. 3, it appears that the 900 K O/C/Mo(110) surface is less active than C/Mo(110), although both the decomposition and the dehydrogenation pathways are still present. On the other hand, the 600 K O/C/Mo(110) surface appears to be nearly inert toward the decomposition or dehydrogenation of cyclohexene, as evidenced by the lack of H_2 evolution, the near absence of benzene desorption, and the intense desorption of molecular cyclohexene. The surface activity and product selectivity will be quantified in Section 4.

HREEL spectra following the decomposition of adsorbed cyclohexene on the 600 and 900 K O/C/Mo(110) surfaces

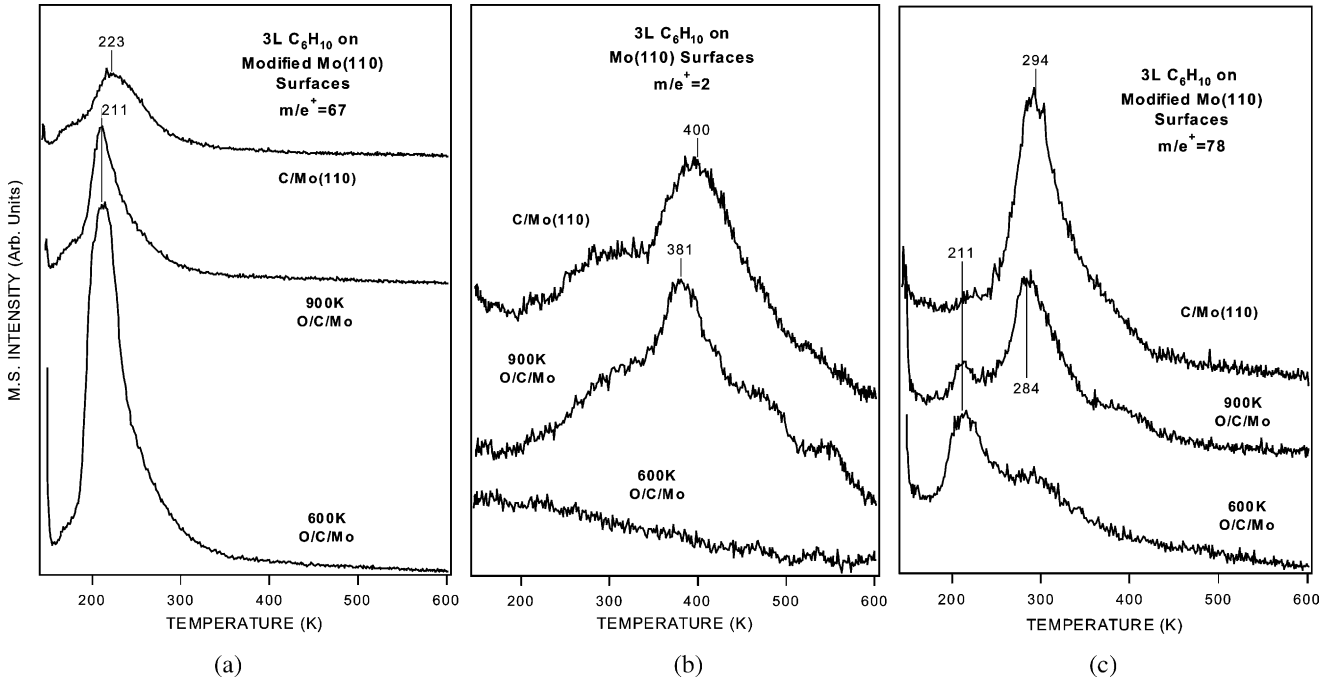

Fig. 3. TPD spectra of (a) cyclohexene, (b) hydrogen, and (c) benzene obtained following 3.0 L exposures of cyclohexene on modified Mo(110) surfaces at 120 K.

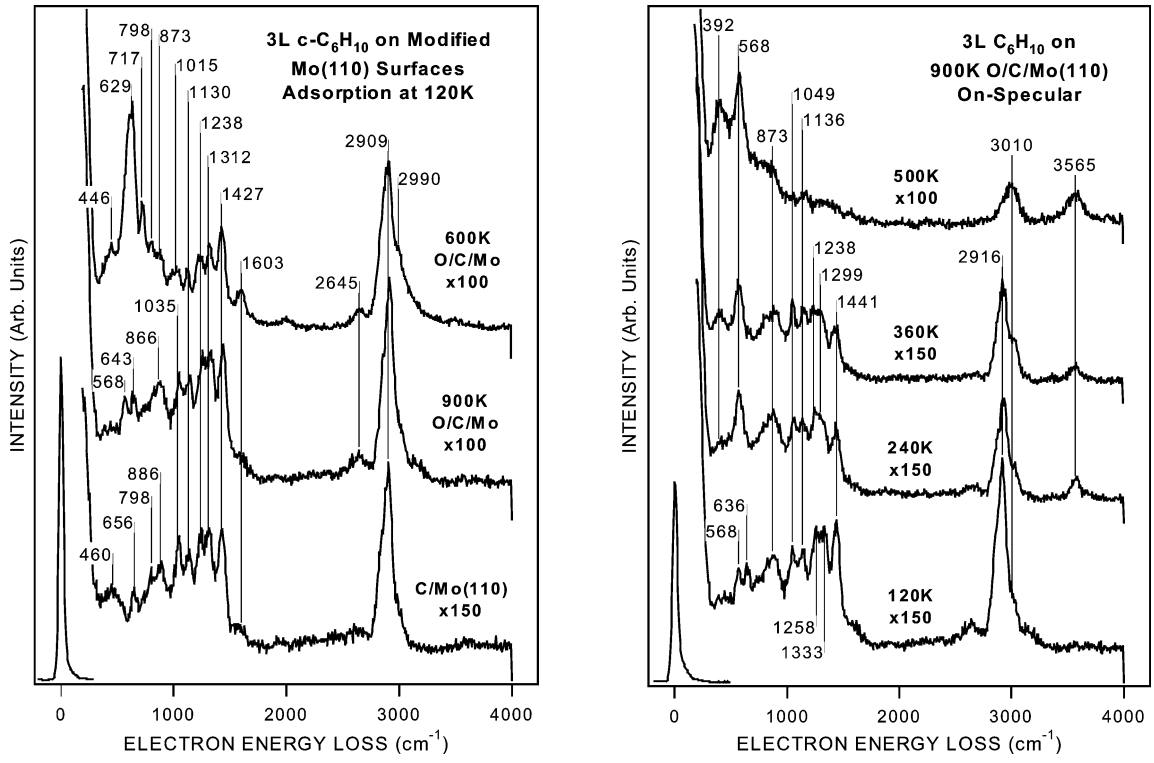

(a) (b)

Fig. 4. (a) HREEL spectra comparing adsorbed cyclohexene on clean and oxygen-modified C/Mo(110) surfaces at 120 K. (b) HREEL spectra monitoring the thermal decomposition of 3.0 L cyclohexene on 900 K O/C/Mo(110) following adsorption at 120 K.

are presented in Fig. 4. The exposures of cyclohexene were made with the crystal temperature at 120 K; the adsorbed layers were then heated to the indicated temperatures and cooled immediately before the HREEL spectra were recorded. Finally, the height of the elastic peaks in all spectra has been normalized to unity, and the indicated expansion factor represents the multiplication factor for each spectrum relative to the elastic peak. The relevant peak frequencies of cyclohexene are assigned in Table 1 [31].

Fig. 4a compares the HREEL spectra recorded after the 120 K adsorption of 3.0 L of cyclohexene on C/Mo(110) and oxygen-modified C/Mo(110). As reported previously [6], cyclohexene adsorbs at 120 K primarily via a di-σ configuration, which is suggested by the detection of a relatively weak ν(C=C) feature at 1603 cm^{-1}. For cyclohexene adsorbed on 600 K O/C/Mo(110), we note that the interactions are nearly identical to cyclohexene adsorbed on the previously examined $p(2 \times 2)$-O/Mo(110) surface [6]. The presence of well-resolved ν(C=C) and δ(C=C) features at 1603 and 717 cm^{-1}, respectively, indicates that the C=C double bond is intact and that cyclohexene interacts weakly with the surface at 120 K. When heated to 240 K and above (spectra not shown), all of the vibrational modes associated with cyclohexene disappear from the 600 K O/C/Mo(110) surface, which corroborates well with the TPD observation that adsorbed cyclohexene desorbs at 211 K.

Table 1
Vibrational assignments for cyclohexene on clean and oxygen-modified C/Mo(110)

Mode	Liquid [31]	C_6H_{10} on C/Mo(110)	C_6H_{10} on 900 K O/C/Mo(110)	C_6H_{10} on 600 K O/C/Mo(110)
Ring deformation	175, 280, 393, 452	460		446
Skeletal distortion	640, 670	656	636	
δ(C=C)	720			717
ν(C–C)	810, 905, 917	798, 886	873	798, 873
ν(C–C) + $\rho(CH_2)$	1038	1035	1049	1015
$\omega(CH_2)$ rock	1138	1130	1136	1130
$\omega(CH_2)$ twist	1241, 1264	1238	1258	1238
$\omega(CH_2)$ wag	1321–1350	1312	1333	1312
$\delta(CH_2)$ scissors	1438–1456	1427	1441	1427
ν(C=C)	1653	1603	1603	1603
ν(–C–H)	2840–2993	2909	2916	2909
ν(=C–H)	3026, 3065			2990

Fig. 4b shows the HREEL spectra monitoring the thermal decomposition of cyclohexene on 900 K O/C/Mo(110). At 120 K, the spectrum is consistent with the presence of di-σ bonded cyclohexene, as assigned by comparing to the HREEL spectra obtained for cyclohexene on C/Mo(110) [6]. The lack of prominent C=C stretching and deformation modes at 1603 and 717 cm^{-1} is the most striking difference when compared with the 600 K O/C/Mo(110) surface. After heating to 240 and then 360 K, the HREEL spectra remain nearly identical to the 120 K spectrum. While there are some minor changes in terms of relative peak intensities, the $\delta(CH_2)$ and $\omega(CH_2)$ features between 1000 and 1450 cm^{-1} all remain in the spectra. In addition, the relatively intense γ(C–H) feature characteristic of adsorbed benzene and expected to appear between 700 and 750 cm^{-1} [6] was not detected at all temperatures. These observations, combined with the fact that gas-phase benzene is detected at 284 K, suggest that the evolution of benzene on the 900 K O/C/Mo(110) surface is a reaction-limited process. At 500 K, the only remaining vibrational modes can be attributed to ν(Mo–C), ν(Mo–O), and $\nu(CH_x)$. The presence of the feature at 3565 cm^{-1} is due to the adsorption and reaction of H_2O from the UHV background during the acquisition of HREEL spectra.

3.2.2. Decomposition of ethylene

The only desorption product resulting from the decomposition of adsorbed ethylene is H_2. Fig. 5 compares the desorption of hydrogen after exposing the modified Mo(110) surfaces to 5.0 L of ethylene at 120 K. Hydrogen desorption from C/Mo(110) is characterized by two peaks, a broader peak at $\sim$ 258 K and a narrower, more intense peak at 393 K. The 900 K O/C/Mo(110) surface only exhibits one broad H_2 desorption feature at $\sim$ 378 K. In contrast, the 600 K O/C/Mo(110) surface does not show any hydrogen peaks, except the initial peak at $\sim$ 150 K related to the desorption from the heating leads. As with the case of cyclohexene, oxygen modification at 600 K deactivates the C/Mo(110) surface; the 900 K O/C/Mo(110) surface, however, appears to retain a significant amount of activity toward the dissociation of ethylene.

HREEL spectra following the adsorption of C_2H_4 at 120 K on the unmodified and oxygen-modified C/Mo(110) are compared in Fig. 6a. The C/Mo(110) spectrum is consistent with previous studies of the presence of strongly adsorbed, di-σ bonded ethylene [5]. However, upon the adsorption onto the 600 K O/C/Mo(110) surface, ethylene appears to be molecularly intact, as evidenced by the symmetric $\omega(=CH_2)$ mode at 940 cm^{-1}, the ν(C=C) mode at 1556 cm^{-1}, and the $\nu(=CH_2)$ mode at 3058 cm^{-1}. The observation of these modes is consistent with the presence of weakly π-bonded C_2H_4 [5,24]. The weaker modes observed at 1197 and 1407 cm^{-1} are associated with the twist and scissor modes of CH_2. The vibrational assignments are summarized in Table 2a [5,32]. When heated to 260 K and above (spectra not shown), all of the ethylene vibrational modes

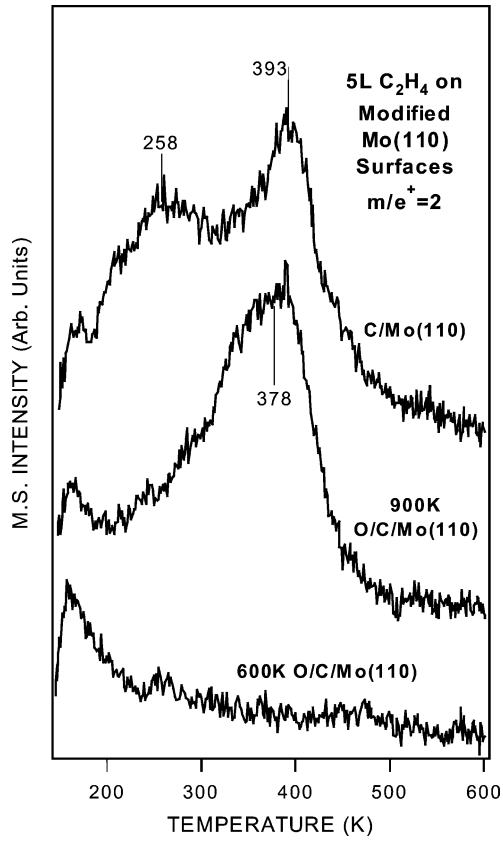

Fig. 5. Hydrogen desorption spectra obtained following 5.0 L exposures of ethylene on modified Mo(110) surfaces at 120 K.

disappear, again agreeing well with the TPD observation that ethylene undergoes reversible adsorption without any detectable amount of decomposition on 600 K O/C/Mo(110).

Fig. 6b shows the HREEL spectra following the thermal decomposition of ethylene on 900 K O/C/Mo(110). At 120 K, the interaction of C_2H_4 with 900 K O/C/Mo(110) is clearly different from that on the 600 K O/C/Mo(110) surface, as indicated by the absence of prominent ν(C=C) and $\nu(=CH_2)$ modes. Vibrational frequencies are observed at 379, 568, 920, 1136, 1387, and 2949 cm^{-1}, which are tentatively assigned to ν(Mo–C), ν(Mo–O), $\omega(CH_2)$-twist, $\omega(CH_2)$-wag, $\omega(CH_2)$-scissor, and $\nu_s(CH_2)$, respectively. The general similarity between the spectra of ethylene on C/Mo(110) and 900 K O/C/Mo(110) suggests that ethylene is also strongly di-σ bonded on the latter surface at 120 K. After heating the overlayer to 260 K, the following spectral changes are observed: (1) the 920, 1136, and 2949 cm^{-1} modes decrease in intensity and (2) the 1387 cm^{-1} mode splits to form two features at 1326 and 1407 cm^{-1}. Though their intensities are rather weak, the 1326 and 1407 cm^{-1} features are the $\delta_s(CH_3)$ and $\delta_{as}(CH_3)$ modes of the ethylidyne intermediate, as identified previously on the unmodified C/Mo(110) surface [5]. The vibrational assignments of the ethylidyne intermediate are summarized in Table 2b [5,33,34]. After heating to 500 K, the only remaining features are at 379 and 568 cm^{-1}, which can be attributed to

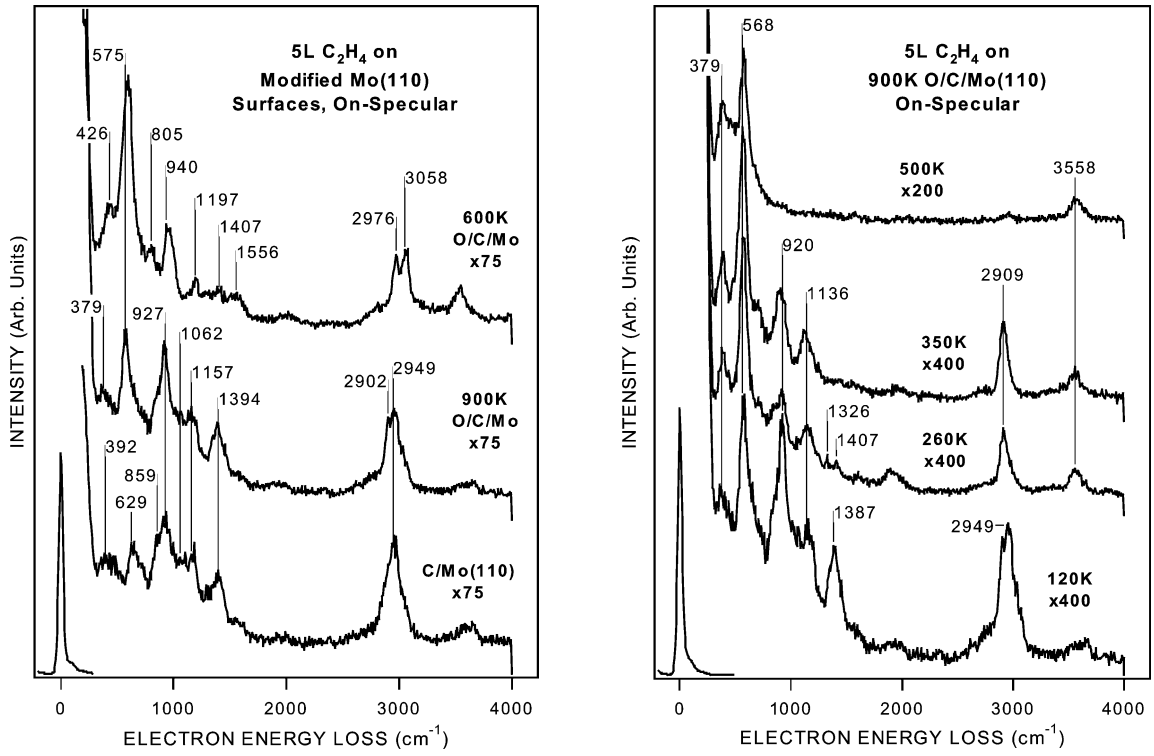

Fig. 6. (a) HREEL spectra comparing adsorbed ethylene on clean and oxygen-modified C/Mo(110) surfaces at 120 K. (b) HREEL spectra monitoring the thermal decomposition of 5.0 L ethylene on 900 K O/C/Mo(110) following adsorption at 120 K.

Table 2a
Vibrational assignments of π-bonded ethylene species

Mode	Gas phase [32]	C_2H_4/O/Mo(110) (5)	C_2H_4/600 K O/C/Mo(110)
$\rho(CH_2)$	826		805
$\omega(CH_2)$	949	965	940
$\tau(CH_2)$	1222	1170	1197
$\delta(CH_2)$	1342	1335	
$\delta(CH_2)$	1444	1420	1407
$\nu(CC)$	1623	1595	1556
$\nu_s(CH_2)$	2989	2975	2976
$\nu_a(CH_2)$	3106	3065	3058

Table 2b
Vibrational assignments of ethylidyne surface intermediate

Mode	$(CH_3C)Co_3(CO)_9$ from IR [33]	C_2H_4/Pt(111) heated to 415 K (34)	C_2H_4/C/Mo(110) heated to 260 K (5)	C_2H_4/900 K O/C/Mo(110) heated to 260 K
$\nu_s(MC)$	401	430	380	379
$\nu_{as}(MC)$	555	600	525	
$\rho(CH_3)$	1004	980	920	920
$\delta_s(CH_3)$	1356	1350	1345	1326
$\delta_{as}(CH_3)$	1420	1420	1430	1407
$\nu(CC)$	1163	1130	1075	1136
$\nu_s(CH_3)$	2888	2890	2915	2909
$\nu_{as}(CH_3)$	2930	2950		

Mo–C and Mo–O vibrations. The presence of the feature at 3558 cm^{-1} is due to the adsorption and reaction of H_2O from the UHV background during the acquisition of HREEL spectra.

3.2.3. Decomposition of methanol

The TPD results from 3.0 L exposure of CH_3OH on the 600 and 900 K O/C/Mo(110) surfaces are compared in Fig. 7, which show the only desorption products, H_2 and

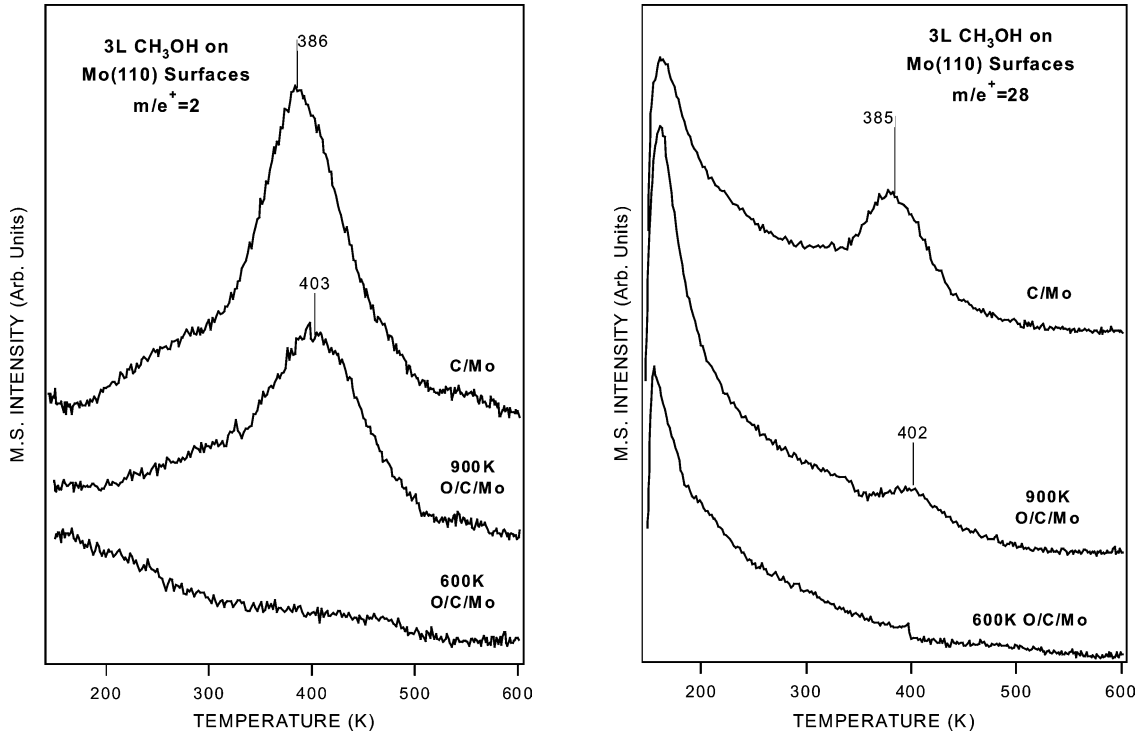

Fig. 7. TPD spectra of (a) hydrogen and (b) carbon monoxide obtained following 3.0 L exposures of methanol on modified Mo(110) surfaces at 120 K.

CO, resulting from the decomposition of methanol. The results from the decomposition of methanol on unmodified C/Mo(110) are also included in the figures for ease of comparison. On 900 K O/C/Mo(110), a single H_2 desorption state is detected at 403 K, along with a very small CO peak at about the same temperature. The absence of masses 15 and 16 (spectra not shown) indicates that no gas-phase methane or methyl radicals are produced from the 900 K O/C/Mo(110) surface. Overall, methanol decomposes on 900 K O/C/Mo(110) to produce gas-phase CO, hydrogen, and surface oxygen and carbon; a more quantitative analysis will be provided in Section 4. In contrast, the TPD results of CH_3OH on 600 K O/C/Mo(110) are distinctly different, as illustrated by the absence of H_2 or CO desorption peaks. Furthermore, no gas-phase HCOH, CO_2, or H_2O products are detected from the two O/C/Mo(110) surfaces (figures not shown).

Fig. 8a shows the HREEL spectra obtained following the adsorption of 3.0 L CH_3OH on C/Mo(110) and O/C/Mo(110). At 120 K, the methoxy intermediate is identified on C/Mo(110) and 900 K O/C/Mo(110), as suggested by the absence of ν(OH) modes between 3200 and 3300 cm^{-1} on these two surfaces. The methoxy vibrational modes are as follows: 1021 cm^{-1}, ν(CO); 1136 cm^{-1}, $\gamma(CH_3)$; 1441 cm^{-1}, $\delta(CH_3)$; 2943 cm^{-1}, $\nu_{as}(CH_3)$. In contrast, the observation of the ν(OH) mode at 3227 cm^{-1} on the 600 K O/C/Mo(110) surface indicates the presence of molecularly adsorbed CH_3OH. When heated to 230 K (spectra not shown), all of the modes associated with the methanol disappear, which is consistent with the lack of dissociation from the TPD results. The vibrational assignments for methanol and methoxy are summarized in Table 3 [16,17,35].

As shown in Fig. 8b, the vibrational modes of adsorbed methanol on 900 K O/C/Mo(110) are observed at 1015, 1143, 1434, and 2956 cm^{-1}, and a CO contamination peak at 1996 cm^{-1}. These features are characteristic of the methoxy intermediate, indicating the cleavage of the O–H bond of methanol at temperatures as low as 120 K. The vibrational assignments of the methoxy (CH_3O) species on 900 K O/C/Mo(110) are summarized in Table 3b. The 230 and 330 K spectra are nearly identical to the 120 K spectrum with the exception of slightly more intense peaks at 379 and 592 cm^{-1}, which are in the frequency range typical for Mo–C and Mo–O modes. Based on these observations, we conclude that the majority of the surface methoxy species are formed at 120 K and remain stable until 330 K. When the adsorbed layer is heated to 450 K, the following changes are observed: (1) the decrease in intensity of modes related to the CH_3 vibrations; (2) the shift of the ν(CO) mode from 1015 to 988 cm^{-1}; (3) the appearance of a strong feature at 592 cm^{-1} which is related to the ν(Mo–O) mode; and (4) the appearance of the ν(OH) mode at 3551 cm^{-1}, which is most likely due to the accumulation and reaction of water from the UHV background during data acquisition. By 600 K, the only features remaining in the spectrum, aside from CO and water contamination, are the Mo–C and Mo–O vibrations at 379 and 592 cm^{-1}, respectively.

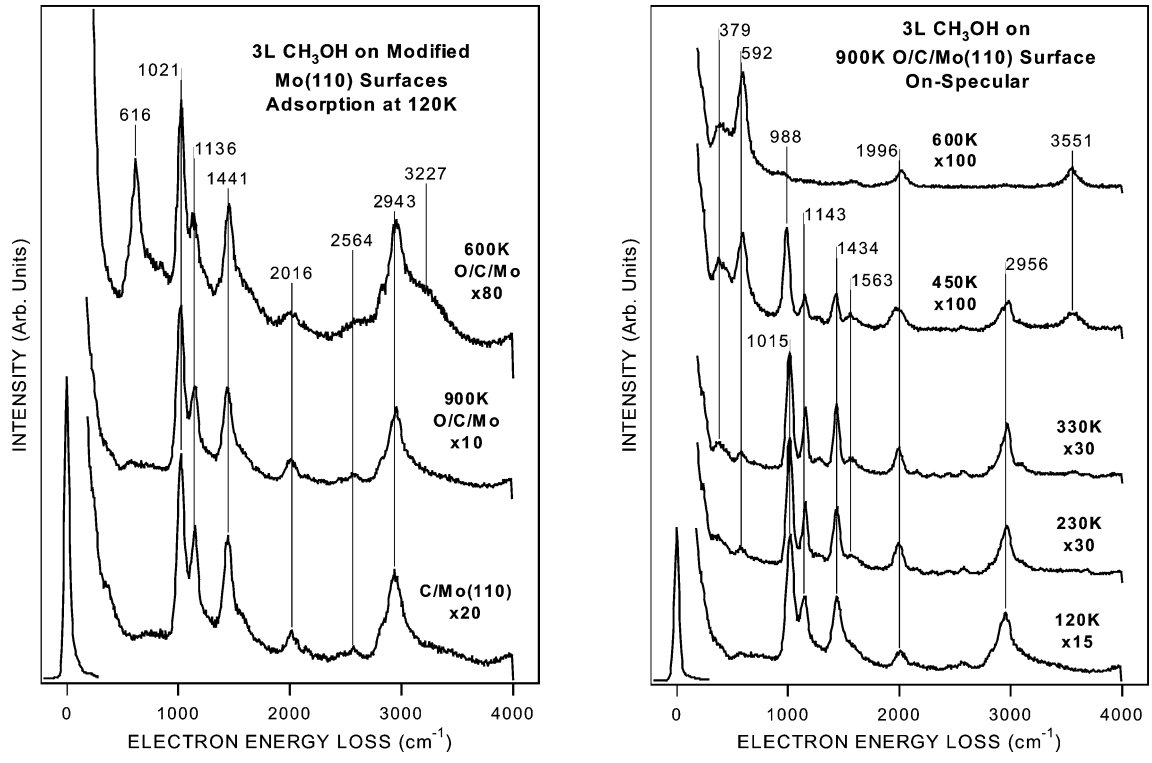

Fig. 8. (a) HREEL spectra comparing adsorbed methanol on clean and oxygen-modified C/Mo(110) surfaces at 120 K. (b) HREEL spectra monitoring the thermal decomposition of 3.0 L methanol on 900 K O/C/Mo(110) following adsorption at 120 K.

It is important to point out that a relatively weak feature is observed at ~ 1563 cm^{-1} in Fig. 8b. This frequency generally corresponds to the ν(C=C) mode of unsaturated hydrocarbons, which might indicate the presence of surface intermediates with unsaturated C=C bonds in addition to the dominant methoxy intermediate. This peak was also detected in our previous studies of methanol on the clean and carbide-modified Mo(110) surfaces [17]. Although the 1563 cm^{-1} feature appears in the frequency range of the ν_{as}(OCO) mode of surface formate [36], the characteristic ν_s(OCO) mode, which is typically the most intense feature in the frequency range of 1350–1380 cm^{-1} [36], is absent in Fig. 8. The absence of this feature suggests that the formate intermediate is not produced during the decomposition of methanol. More detailed studies are necessary to identify the origin of the ~ 1563 cm^{-1} mode.

3.3. *Electronic properties of C/Mo(110) and O/C/Mo(110) surfaces*

In order to better understand the role of oxygen in surface reactivity, we have investigated the electronic properties of unmodified C/Mo(110) and O/C/Mo(110) surfaces using SXPS and NEXAFS. The SXPS valence state spectra comparing the various modified Mo(110) surfaces are shown in Fig. 9. For the C/Mo(110) surface, the valence state is characterized by two overlapping peaks at ~ 5.7 and ~ 1.9 eV, which are related to emissions from the p–σ and p–π band, respectively [25,26]. The detection of these broad features, as well as the presence of a relatively weak feature at approximately ~ 12.5 eV, agrees well with previous studies of carbon-modified Mo surfaces. Additionally, the lack of a well-defined Fermi edge is also consistent with previous investigations [25]. Upon oxygen modification at 600 and 900 K, the peak at ~ 5.7 eV increases in intensity relative to the ~ 1.9 eV peak. For comparison, the ~ 12.5 eV feature of 900 K O/C/Mo(110) decreases in intensity when compared to the 600 K O/C/Mo(110) and C/Mo(110) surfaces. This observation corroborates with TPD and AES measurements showing the removal of a fraction of surface carbon upon exposure to oxygen at 900 K. Overall, aside from the feature at ~ 12.5 eV, the valence states of both O/C/Mo(110) surfaces closely resemble those of the O/Mo(110) surface.

In order to compare the local bonding environment of carbon atoms in the unmodified and oxygen-modified C/Mo(110), we have performed NEXAFS measurements of the C K-edge features. Fig. 10 compares the NEXAFS spectra of C/Mo(110) and 900 K O/C/Mo(110). The NEXAFS spectra of C/Mo(110) recorded at the 30° glancing incidence, as shown in Fig. 10a, are characterized by three features at approximately 284.4, 286.4, and 288.0 eV. Based on comparisons with previous NEXAFS investigations of carbide surfaces [2,19,27,28], these resonances can be assigned to the transitions of C (1s) electrons to the unoccupied p–d hybridized states of molybdenum carbide [2,19].

Table 3a
Vibrational frequencies (cm^{-1}) of solid phase CH_3OH and molecular CH_3OH adsorbed on various oxygen-modified surfaces

Mode	CH_3OH (s) [35]	CH_3OH/O/W(111) [16]	CH_3OH/O/W(110) [16]	Multilayer/C/Mo(110) [17]	CH_3OH/600 K O/C/Mo(110)
δ(OH)	730	778	758	771	
ν(CO)	1032	1062	1042	1028	1021
$\gamma(CH_3)$	1124	1143	1143	1136	1136
$\delta(CH_3)$	1452	1488	1461	1468	1441
$\nu_s(CH_3)$	2828		2841		
$\nu_{as}(CH_3)$	2951	2990	2956	2929	2943
ν(OH)	3225	3288	3267	3261	3227

Table 3b
Vibrational frequencies (cm^{-1}) of methoxy (CH_3O) on C/Mo(110) and 900 K O/C/Mo(110)

Mode	CH_3O/C/W(111) [16]	CH_3O/C/W(110) [16]	CH_3O/C/Mo(110)	CH_3O/900 K O/C/W(110)
ν(M–O)	534	561		
ν(CO)	1021	994	1021	1015
$\gamma(CH_3)$	1157	1157	1136	1143
$\delta(CH_3)$	1448	1448	1441	1434
$\nu_s(CH_3)$				
$\nu_{as}(CH_3)$	2956	2943	2943	2956

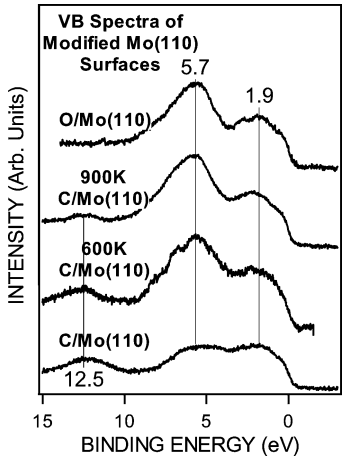

Fig. 9. Comparison of SXPS spectra of valence states of modified Mo(110) surfaces.

Overall, the peak positions of the C *K*-edge features are very similar between the unmodified C/Mo(110) and 900 K O/C/Mo(110) surfaces. Since the lineshape and peak positions of the C *K*-edge features are very sensitive to the bonding environment of carbon atoms [19], the comparison in Fig. 10 suggests that carbon atoms remain bonded to similar sites on the C/Mo(110) and 900 K O/C/Mo(110) surfaces, which might be responsible for the general similarities in the chemical properties between the two surfaces.

Furthermore, the comparison of Fig. 10a (glancing incidence) and Fig. 10b (normal incidence) shows that the C *K*-edge features have strong polarization dependence on both C/Mo(110) and 900 K O/C/Mo(110). Because carbon atoms residing at below the metal surface would show an isotropic distribution [19], the observation of a strong polarization dependence suggests that at least a fraction of carbon atoms is occupying the surface sites in both C/Mo(110) and 900 K O/C/Mo(110).

4. Discussion

4.1. Surface activity and product selectivity

4.1.1. Decomposition of cyclohexene

In this section we will provide quantitative analysis of the surface reactivity and product selectivity of the 600 and 900 K O/C/Mo(110) surfaces. These values are derived by comparing the TPD peak areas with corresponding AES measurements, as described in detail for other surfaces [11,16,17]. As described in earlier publications, the activity and selectivity values were typically obtained from at least two sets of TPD and AES measurements, with typical errors bars being less than 10%. Because of the difficulty in drawing baselines in some of the current TPD measurements (for example, Fig. 5), we anticipate that the error bars might be larger for these measurements. Nonetheless we feel that it is important to provide a quantitative analysis for ease of comparison with previous work on other surfaces

The TPD results in Fig. 3 reveal the following two reactions of cyclohexene on C/Mo(110) and 900 K O/C/Mo(110):

$$m \cdot c - C_6H_{10} \rightarrow 6m \cdot C + 5m \cdot H_2, \quad (1)$$

$$n \cdot c - C_6H_{10} \rightarrow n \cdot C_6H_6 + 2n \cdot H_2. \quad (2)$$

By combining AES ratios with TPD peak areas, the values of m and n were calculated, from our previous studies on C/Mo(110), to be ~ 0.017 (30%) and ~ 0.039 (70%) cyclohexene molecules per Mo atom, respectively. The overall activity, defined as $m + n$, is therefore 0.056 cyclohexene molecules per Mo atom [6,7]. To determine the product selectivity of cyclohexene on the 900 K O/C/Mo(110) surface, one needs to compare the hydrogen and benzene peak areas to those of C/Mo(110). Using Eqs. (1) and (2) and the

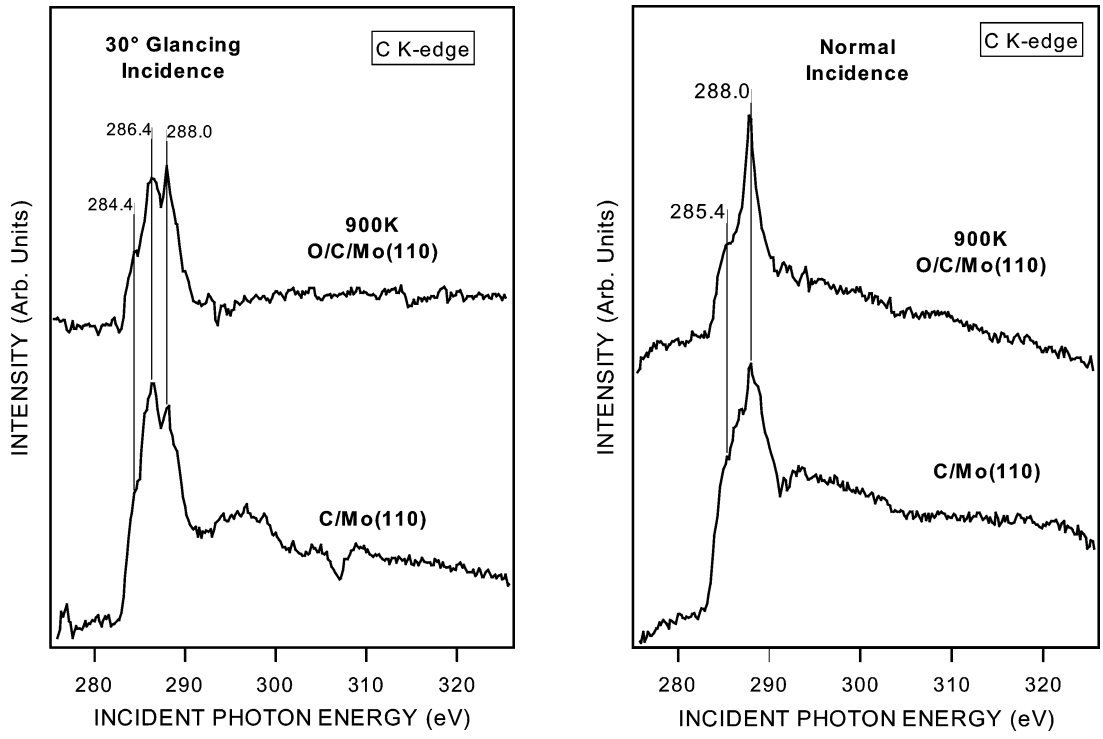

Fig. 10. Normal (a) and glancing (b) incidence carbon K-edge NEXAF spectra of C/Mo(110) and 900 K O/C/Mo(110).

known activity values on C/Mo(110), the following relationships can be written:

$$\frac{\text{Area}_{\text{Benzene}}^{\text{O(900 K)/C/Mo(110)}}}{\text{Area}_{\text{Benzene}}^{\text{C/Mo(110)}}} = \frac{n}{0.039} = 0.37 \quad \Rightarrow \quad n \approx 0.014, \tag{3}$$

$$\frac{\text{Area}_{\text{H}_2}^{\text{O(900 K)/C/Mo(110)}}}{\text{Area}_{\text{H}_2}^{\text{C/Mo(110)}}} = \frac{2n+5m}{2(0.039)+5(0.017)} = 0.85$$

$$\Rightarrow \quad m \approx 0.022. \tag{4}$$

The overall cyclohexene activity on the 900 K O/C/Mo(110) surface is estimated to be ~ 0.036 molecules per Mo atom, with 61% completely decomposing and 39% dehydrogenating to benzene. A summary of these results is presented in Table 4a.

In contrast, aside from molecular cyclohexene, no other gas-phase products were observed on the 600 K O/C/Mo(110), indicating the inert nature of this surface.

4.1.2. Decomposition of ethylene

In the previous investigation involving the decomposition of ethylene on clean and carbide-modified Mo(110), it was determined that gas-phase hydrogen and surface carbon were the only products after the TPD measurements [5]. The decomposition pathway for ethylene on these surfaces is therefore:

$$x \cdot \text{C}_2\text{H}_4 \xrightarrow{\Delta} 2x \cdot \text{C} + 2x \cdot \text{H}_2. \tag{5}$$

The decomposition activity of ethylene on clean Mo(110) was previously calculated to be ~ 0.15 ethylene molecules per Mo atom. The C/Mo(110) surface was observed to retain $\geqslant 80\%$ of the decomposition activity compared to clean Mo(110) [5].

In this study, we confirmed that ~ 0.15 ethylene molecules per Mo atom decomposes on clean Mo(110), based on AES ratios after TPD measurements (spectra not shown). By comparing the relative intensities of hydrogen desorption, we can then determine that ~ 0.13 and ~ 0.12 ethylene molecules per Mo atom dissociate on the C/Mo(110) and the 900 K O/C/Mo(110) surfaces, respectively,

$$\frac{\text{Area}_{\text{H}_2}^{\text{C/Mo(110)}}}{\text{Area}_{\text{H}_2}^{\text{Mo(110)}}} = 0.86 \quad \Rightarrow \quad \text{Activity}_{\text{C}_2\text{H}_4}^{\text{C/Mo(110)}} \approx 0.13, \tag{6}$$

$$\frac{\text{Area}_{\text{H}_2}^{\text{O/C/Mo(110)}}}{\text{Area}_{\text{H}_2}^{\text{Mo(110)}}} = 0.80 \quad \Rightarrow \quad \text{Activity}_{\text{C}_2\text{H}_4}^{\text{O/C/Mo(110)}} \approx 0.12. \tag{7}$$

On the 600 K O/C/Mo(110) surface, no hydrogen desorption is detected, and thus the decomposition activity is zero. These values are compared in Table 4b.

4.1.3. Decomposition of methanol

On both C/Mo(110) and 900 K O/C/Mo(110), hydrogen and CO are the gas-phase products, and atomic carbon and oxygen are the remaining surface species after TPD mea-

Table 4a
Reaction pathways of cyclohexene on C/Mo(110) and 900 K O/C/Mo(110)

Surface	C_6H_6 activity: cyclohexene per metal atom (% selectivity)	Complete decomposition activity: cyclohexene per metal atom (% selectivity)	Overall activity: cyclohexene per metal atom
C/Mo(110) (6, 7)	0.035 (70)	0.015 (30)	0.050
900 K O/C/Mo(110)	0.014 (39)	0.022 (61)	0.036
C/W(111) (8)	0.059 (67)	0.029 (33)	0.088
900 K O/C/W(111) (9)	0.054 (83)	0.011 (17)	0.065
750 K C/Ti(0001) (12)	0.084 (50)	0.084 (50)	0.168
750 K O/C/Ti(0001) (12)	0.139 (90)	0.015 (10)	0.154

Table 4b
Activity of C/Mo(110) and 900 K O/C/Mo(110) toward ethylene decomposition

Surfaces	Activity (ethylene molecules per metal atom)
C/Mo(110)	0.130
900 K O/C/Mo(110)	0.120
C/W(110) (11)	0.104
C/W(111) (11)	0.145
C/Ti(0001) (12)	0.250

surements to 600 K. The reaction pathways are therefore:

$$x\mathrm{CH_3OH} \xrightarrow{\Delta} x\mathrm{C}(a) + x\mathrm{O}(a) + 2x\mathrm{H_2}(g), \tag{8}$$

$$y\mathrm{CH_3OH} \xrightarrow{\Delta} y\mathrm{CO}(g) + 2y\mathrm{H_2}(g). \tag{9}$$

To estimate the product yields on the 900 K O/C/Mo(110) surface, one can simply determine the hydrogen and CO TPD peak areas relative to those from C/Mo(110). The activity of C/Mo(110) toward the complete decomposition of methanol, x, and the production of gas-phase CO, y, were previously estimated to be 0.142 and 0.083 molecules per Mo atom, respectively [17]. By comparing the H_2 and CO peak areas of the 900 K O/C/Mo(110) surface to those of C/Mo(110), the selectivity x' and y' can be determined:

$$\frac{2(x+y)}{2(x'+y')} = \frac{\mathrm{Area}_{\mathrm{H_2}}^{\mathrm{C/Mo(110)}}}{\mathrm{Area}_{\mathrm{H_2}}^{\mathrm{O/C/Mo(110)}}} = \frac{2(0.142+0.083)}{2(x'+y')}$$
$$\approx 1.81 \quad \Rightarrow \quad x'+y' = 0.124, \tag{10}$$

$$\frac{y}{y'} = \frac{\mathrm{Area}_{\mathrm{CO}}^{\mathrm{C/Mo(110)}}}{\mathrm{Area}_{\mathrm{CO}}^{\mathrm{O/C/Mo(110)}}}[@\mathrm{Temp} < 600\ \mathrm{K}] = \frac{0.083}{y'}$$
$$\approx 4.23 \quad \Rightarrow \quad y' = 0.020. \tag{11}$$

As estimated from Eqs. (10) and (11), the overall decomposition activity on the 900 K O/C/Mo(110) surface ($x'+y'$) is 0.124 methanol molecules per Mo atom, and that ~ 84% of the methanol completely decomposes while 16% reacts to produce gas-phase CO and H_2. A summary of the methanol activity and product selectivity is shown in Table 4c.

4.2. Possible origin of different activities of 600 and 900 K O/C/Mo(110) surfaces

As quantified in Section 4.1 and summarized in Tables 4a–4c, the 900 K O/C/Mo(110) surface remains active toward the dissociation of cyclohexene, ethylene, and methanol. In contrast, the 600 K O/C/Mo(110) surface is essentially chemically inert. The following differences and similarities exist for the two O/C/Mo(110) surfaces:

(1) The two surfaces have different atomic C/Mo and O/Mo ratios, with approximately 0.36 and 0.44 for 600 K O/C/Mo(110) and 0.31 and 0.08 for 900 K O/C/Mo(110) (Section 2.2).
(2) The vibrational frequency for the ν(Mo–O) stretching mode (Fig. 1) is different, at 595 cm^{-1} for 600 K O/C/Mo(110) and 561 cm^{-1} for 900 K O/C/Mo(110), suggesting different binding environments for oxygen on the two surfaces.
(3) The SXPS measurements (Fig. 9) reveal similar electronic valence states for the two surfaces, suggesting that the different activities of the two surfaces did not result from different electronic modifications by oxygen.

We attempt to explain the different activities of the two O/C/Mo(110) surfaces using the schematic surface structure models shown in Fig. 11. As noted earlier, the unmodified C/Mo(110) surface is characterized by an AES atomic C/Mo ratio in the range of 0.40 to 0.46, which is close to the Mo_2C stoichiometry of bulk molybdenum carbides. Fig. 11a and 11b show the two possible surface structures of Mo_2C

Table 4c
Product yields of methanol on C/Mo(110) and 900 K O/C/Mo(110)

Surfaces	Complete decomposition activity per metal atom (%)	CO activity per metal atom (%)	CH_4 activity per metal atom (%)	Total # of CH_3OH reacting per metal atom
C/Mo(110) (17)	0.142 (63)	0.083 (37)	0 (0)	0.225
900 K O/C/Mo(110)	0.104 (84)	0.020 (16)	0 (0)	0.124
C/W(111) (16)	0.155 (55)	0.087 (31)	0.038 (14)	0.280
900 K O/C/W(111) (16)	0.050 (21)	0.160 (68)	0.026 (11)	0.236

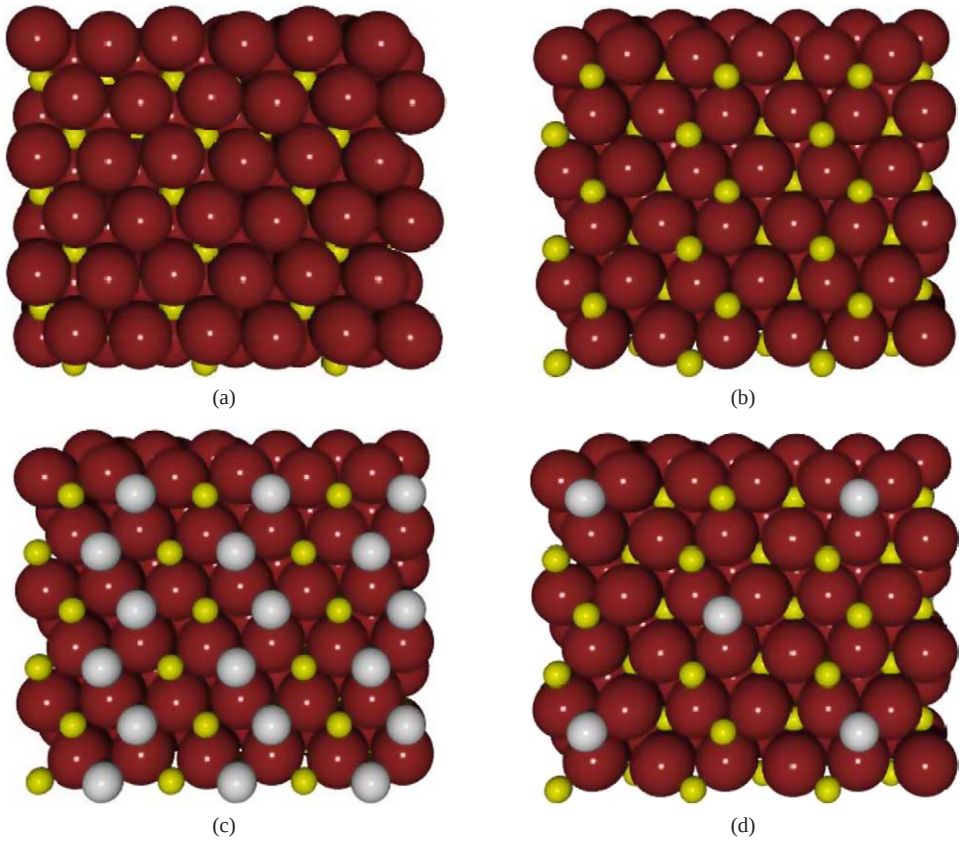

Fig. 11. Schematic illustration of (a) Mo-terminated Mo_2C surface, (b) C-terminated Mo_2C surface, (c) 600 K O/C/Mo(110) surface, and (d) 900 K O/C/Mo(110) surface.

that are terminated by Mo and by C, respectively [29]. Because the NEXAFS results (Fig. 10) show a strong polarization dependence in the C *K*-edge features, we believe that the C-terminated surface should be more representative of the C/Mo(110) surface.

Fig. 11c and 11d illustrate the potential surface structures of the 600 and 900 K O/C/Mo(110) surfaces, respectively. As shown in the TPD spectra in Fig. 2, the recombination of atomic C and O, to gas-phase CO, does not occur until ∼ 700 K. Therefore, exposing C/Mo(110) to oxygen at 600 K should not remove surface C atoms. In this case the O atoms should occupy the remainder surface sites, as illustrated in Fig. 11c, making this surface chemically inert due to the blocking of surface sites. On the other hand, exposing C/Mo(110) to oxygen at 900 K should start to remove a fraction of surface C atoms by oxygen due to the recombinative CO desorption. In this case some of the O atoms could reside on the surface sites that are previously occupied by C, as illustrated in Fig. 11d. This surface should remain chemically active due to the availability of the surface reactive sites. Although the stoichiometries in Fig. 11, Mo_2C for C/Mo(110), Mo_2C–O for 600 K O/Mo(110), and $Mo_2C_{0.75}$–$O_{0.25}$ for 900 K O/C/Mo(110), are slightly off from the atomic ratios derived from the AES measurements, these structures provide a qualitative, self-consistent explanation to interpret the chemical and spectroscopic results in the current paper. Density functional theory (DFT) modeling studies to determine the electronic properties of carbide and oxycarbide structures in Fig. 11 are underway. The initial results provide an excellent agreement between the DFT modeling and the SXPS results for the Mo(110) and C/Mo(110) surfaces, and will be presented in a separate paper [30].

It is important to point out that the SXPS results presented here are not sensitive enough to distinguish minor differences in electronic structures if some oxygen dissolves into the subsurface at 900 K. Similarly, although the polarization-dependent NEXAF spectrum reveals the presence of surface oxygen, it again does not rule out the possibility of a fraction of oxygen residing in the subsurface at 900 K. One potential way to determine the presence of subsurface oxygen is to more accurately interpret the HREELS data in Fig. 1, where one would expect different ν(Mo–O) frequencies for oxygen residing in the surface and subsurface. We are currently performing DFT modeling to help the vibrational assignment of the HREELS spectra of the 600 and 900 K O/C/Mo(110) surfaces.

4.3. Comparing O/C/Mo(110) with oxygen-modified C/W(111) and C/Ti(0001)

As summarized in Table 4a, the selective dehydrogenation of cyclohexene can be used as a probe to compare O/C/Mo(110) with other oxygen-modified carbide surfaces.

When comparing the effects of oxygen modification on C/Mo(110) and C/W(111), one notices both differences and similarities. While both C/Mo(110) and C/W(111) were deactivated by exposure to oxygen at 600 K, oxygen modification at 900 K appeared to have different effects on C/Mo(110) and C/W(111). In both cases, oxygen modification at 900 K decreased the overall activity toward cyclohexene by nearly 30%. The selectivity toward benzene production was reduced from 70% on C/Mo(110) to 39% on 900 K O/C/Mo(110). In contrast, the 900 K O/C/W(111) surface actually showed a higher selectivity (83%) toward the production of benzene than unmodified C/W(111) (67%) [8,9]. We have also recently completed parallel studies of the dehydrogenation of cyclohexene on unmodified and oxygen-modified C/Ti(0001) [12]. When modified by oxygen at 750 K, the selectivity toward benzene increased from 50 to 90% on O/C/Ti(0001) [12]. These comparisons show that the effect of oxygen modification depends not only on the oxygen adsorption environment, but also on the identity and/or structure of the metal substrates. More systematic experimental and theoretical studies are necessary to establish a general trends in the chemical properties of oxycarbides of different metals.

5. Conclusions

Based on the results and discussion presented above, the following conclusions can be made regarding the modification effect of oxygen on C/Mo(110):

(1) The surface activities of O/C/Mo(110) surfaces depend strongly on the temperature at which oxygen is exposed to C/Mo(110). While the 900 K O/C/Mo(110) surface remains active toward the dissociation of cyclohexene, ethylene, and methanol, the 600 K O/C/Mo(110) surface is essentially inert.
(2) The different activities are most likely related to the different binding environments of the O atoms on C/Mo(110), as illustrated in Fig. 11: Upon exposing C/Mo(110) to 600 K, which is below the onset temperature for the recombinative desorption of CO, the O atoms most likely occupy the active surface sites of C/Mo(110), thus deactivating the surface. On the other hand, exposing C/Mo(110) at 900 K leads to the removal of a fraction of C atoms due to recombinative CO desorption. The resulting O/C/Mo(110) surface will most likely retain the active surface sites for reactions toward olefins and oxygenates.
(3) Comparisons with other oxygen-modified carbide surfaces indicate the complex nature of oxygen modification. Systematic experimental and DFT modeling is required to identify general trends in the reactivities of oxycarbides.

Acknowledgments

We acknowledge financial support from Basic Energy Sciences of the Department of Energy (DOE/BES Grant DE-FG02-04ER15501). We thank Dr. D.R. Mullins of Oak Ridge National Laboratory and Dr. P.A. Stevens of ExxonMobil for technical assistance at the National Synchrotron Light Source U12A and U1A beamlines, respectively. H.H.H. acknowledges financial support from the Presidential Fellowship at the University of Delaware and the American Vacuum Society Graduate Fellowship. M.B.Z. acknowledges partial financial support from a National Aeronautics and Space Administration Fellowship. We thank J.R. Kitchin for helpful discussion and assistance in preparing Fig. 11.

References

[1] S.T. Oyama, The Chemistry of Transition Metal Carbides and Nitrides, Blackie Academic and Professional, Glasgow, 1996.
[2] J.G. Chen, Chem. Rev. 96 (1996) 1477.
[3] J.G. Chen, M.D. Weisel, Z.-M. Liu, J.M. White, J. Am. Chem. Soc. 115 (1993) 8876.
[4] J.G. Chen, J. Catal. 154 (1995) 80.
[5] B. Fruhberger, J.G. Chen, J. Am. Chem. Soc. 118 (1996) 11,599.
[6] J. Eng Jr., B.E. Bent, B. Fruhberger, J.G. Chen, Langmuir 14 (1998) 1301.
[7] J. Eng Jr., J.G. Chen, Surf. Sci. 414 (1998) 374.
[8] N. Liu, S.A. Rykov, H.H. Hwu, M.T. Buelow, J.G. Chen, J. Phys. Chem. B 105 (2001) 3894.
[9] N. Liu, S.A. Rykov, J.G. Chen, Surf. Sci. 487 (2001) 107.
[10] M.H. Zhang, et al., Catal. Lett. 77 (2001) 29;
M.H. Zhang, et al., Surf. Sci. 522 (2003) 112.
[11] H.H. Hwu, J.G. Chen, J. Phys. Chem. B 107 (2003) 11,467.
[12] H.H. Hwu, J.G. Chen, Surf. Sci. 557 (2004) 144.
[13] E. Iglesia, F.H. Ribeiro, M. Boudart, J.E. Baumgartner, Catal. Today 15 (1992) 455;
E. Iglesia, F.H. Ribeiro, M. Boudart, J.E. Baumgartner, Catal. Today 15 (1992) 307.
[14] E. Iglesia, J.E. Baumgartner, F.H. Ribeiro, M. Boudart, J. Catal. 131 (1991) 523;
F.H. Ribeiro, M. Boudart, R.A. Dallabetta, E. Iglesia, J. Catal. 130 (1991) 498.
[15] C. Pham-Huu, M.J. Ledoux, J. Guille, J. Catal. 143 (1993) 249;
E.A. Blekkan, C.C. Pham-Huu, M.J. Ledoux, J. Guille, Ind. Eng. Chem. Res. 33 (1994) 1657.
[16] H.H. Hwu, J.G. Chen, K. Kourtakis, G. Lavin, J. Phys. Chem. B 105 (2001) 10,037;
H.H. Hwu, J.G. Chen, J. Phys. Chem. B 107 (2003) 2029.
[17] H.H. Hwu, J.G. Chen, Surf. Sci. 536 (2003) 75.
[18] D.R. Mullins, P.V. Radulovic, S.H. Overbury, Surf. Sci. 429 (1999) 186.
[19] J.G. Chen, Surf. Sci. Rep. 30 (1997) 1.
[20] K.D. Childs, et al., The Handbook of Auger Electron Spectroscopy, third ed., Physical Electronics, 1995.
[21] J. DiNardo, G.B. Blanchet, E.W. Plummer, Surf. Sci. 140 (1984) L229.
[22] H. Froitzheim, H. Ibach, S. Lewald, Phys. Rev. B 14 (1976) 1362.
[23] P.K. Stefanov, T.S. Marinova, Surf. Sci. 200 (1988) 26.
[24] H. Ibach, D.L. Mills, Electron Energy Loss Spectroscopy and Surface Vibrations, Academic Press, New York, 1982.

[25] P. Reinke, P. Oelhafen, Surf. Sci. 468 (2000) 203;
P. Reinke, P. Oelhafen, J. Appl. Phys. 81 (1997) 2396.
[26] S. Schelz, P. Kania, P. Oelhafen, H.-J. Guntherodt, T. Richmond, Surf. Sci. 359 (1995) 227.
[27] J.G. Chen, J. Eng Jr., S.P. Kelty, Catal. Today 43 (1998) 147.
[28] B. Fruhberger, J.G. Chen, J. Eng Jr., B.E. Bent, J. Vac. Sci. Technol. A 14 (1996) 1475.
[29] Dopovidi Akademii Nauk Ukrains'koi RSR, Seriya A: Fiziko-Tekhnichni ta Matematichni Nauki (3) (1991) 78–82.
[30] J.R. Kitchin, J.K. Norskov, M.A. Barteau, J.G. Chen, Catal. Today (2004) submitted.
[31] M.A. Newton, C.T. Campbell, Z. Phys. Chem. 198 (1997) 169.
[32] G. Herzberg, Molecular Spectra and Molecular Structure, vol. II, Krieger, Malabar, FL, 1991.
[33] P. Skinner, et al., J. Chem. Soc., Faraday II 77 (1981) 685.
[34] H. Steininger, H. Ibach, S. Lehwald, Surf. Sci. 117 (1982) 685.
[35] M. Falk, E. Whalley, J. Chem. Phys. 34 (1961) 1554.
[36] J.E. Crowell, J.G. Chen, J.T. Yates Jr., J. Chem. Phys. 85 (1986) 3111.